Microwave response of anisotropic magnetorheological elastomers: Model and experiments

A. Butera* and N. Álvarez
Centro Atómico Bariloche (CNEA) and Instituto Balseiro (U. N. Cuyo), 8400 Bariloche, Río Negro, Argentina

G. Jorge
Departamento Física, Facultad de Ciencias Exactas y Naturales, Universidad de Buenos Aires, Argentina

M. M. Ruiz, J. L. Mietta, and R. M. Negri
INQUIMAE, Facultad de Ciencias Exactas y Naturales, Universidad de Buenos Aires, Argentina
(Received 10 August 2012; published 31 October 2012)

We present ferromagnetic resonance measurements of Fe_3O_4 nanoparticles which have been dispersed in an elastomeric polymer [polydimethylsiloxane (PDMS)] at two different concentrations (5% and 15% w/w), and then cured in the presence of a uniform magnetic field. With this procedure it is possible to align the particles forming unidimensional needlelike cylindrical agglomerates with a relatively high length/diameter ratio. The dynamical response of this nanostructured composite has been characterized using ferromagnetic resonance at K band (24 GHz) and Q band (34 GHz). In both cases we have observed an anisotropic behavior in the resonance field when the external magnetic field is rotated from the direction of the needles to the perpendicular plane. However, the measured variation is considerably lower than the values expected for an array of perfectly homogeneous long cylinders in which the elongated shape causes a uniaxial anisotropy. Results have been analyzed using the standard Smit and Beljers formalism, considering a phenomenological shape factor, P, that accounts for the reduced anisotropy. Also an ellipticity factor in the cross section of the needles, r, and Gaussian fluctuations of the shape factor, σP, are needed to explain the observed angular variation of the linewidth. The values of these parameters are consistent with data obtained at K and Q bands, supporting the proposed model, although some differences have been found for the two studied concentrations.

DOI: 10.1103/PhysRevB.86.144424 PACS number(s): 76.50.+g, 75.30.Gw, 75.75.−c, 75.50.Tt

I. INTRODUCTION

Iron oxides, and particularly magnetite (Fe_3O_4), have been extensively studied since research in magnetic materials started. Magnetite crystallizes in a spinel structure and orders ferrimagnetically below 840 K with a saturation magnetization $M_s \sim 480$ emu/cm^3 when in bulk form.[1] This material was also studied in systems with reduced dimensions, particularly nanoparticles,[2–4] thin films,[5] and structured multilayers[6] in order to induce new magnetic characteristics, absent in bulk samples. These engineered materials, with novel magnetic properties, open a broad spectrum of new potential applications. One of these engineered systems consists in the preparation of magnetorheological elastomers (MRE), in which magnetic nanoparticles are dispersed in an organic elastic matrix and then cured in the presence of an external applied field in order to induce anisotropic transport and magnetic properties. These elastomeric polymers are very attractive due to their potential use in flexible electronics, including pressure and magnetic field sensors. For these applications oxide nanoparticles (typically Fe_3O_4 or $CoFe_2O_4$) are agglomerated and then covered with a metallic shell, such as Ag, forming a core/shell structure of micrometer size.[7,8] When the particles are introduced in a polymer matrix and then cured in the presence of a magnetic field, they tend to align in the shape of needlelike elongated cylinders with a morphological length/diameter aspect ratio in the range of 100, which is responsible for the observed anisotropic magnetic response.

We have performed a detailed study using ferromagnetic resonance (FMR) techniques in order to get a deeper understanding of the observed magnetic behavior and correlate these results with the microstructure of the composite. This technique is specially suitable for the determination of magnetic anisotropies and the distribution of magnetic parameters, through the analysis of the resonance field, the linewidth, and the line shape.

II. EXPERIMENTAL DETAILS

The synthesis of the magnetic particles and the preparation of the MRE was explained in detail in Ref. 7. Briefly, Fe_3O_4 nanoparticles were obtained by chemical coprecipitation of a solution of hydrated $FeCl_3$ and $FeCl_2$ in HCl mixed with NaOH. After several steps of washing and centrifugation, it was possible to obtain magnetite nanoparticles of the correct crystalline phase with an average diameter of 13 nm and a relatively narrow size distribution. The particles were then dispersed in a polydimethylsiloxane (PDMS) matrix and cured at 75 °C for 4 h in the presence of a uniform dc magnetic field of 3000 Oe. As already mentioned, the magnetite nanoparticles tend to agglomerate forming needlelike cylinders. Two different dispersions, 5% and 15% w/w Fe_3O_4 in PDMS, were prepared to account for possible effects of interactions among needles. The average diameter, length, and separation among cylinders is 51 μm, 3 mm, 100 μm for Fe_3O_4:PDMS 15%, and 20 μm, 3 mm, 120 μm for Fe_3O_4:PDMS 5%. As can be seen in Fig. 1 (and in more detail in Fig. 4 of Ref. 7) the cylinders have a granular texture and their cross section is generally elliptical with a transverse aspect ratio that can be higher than 2.

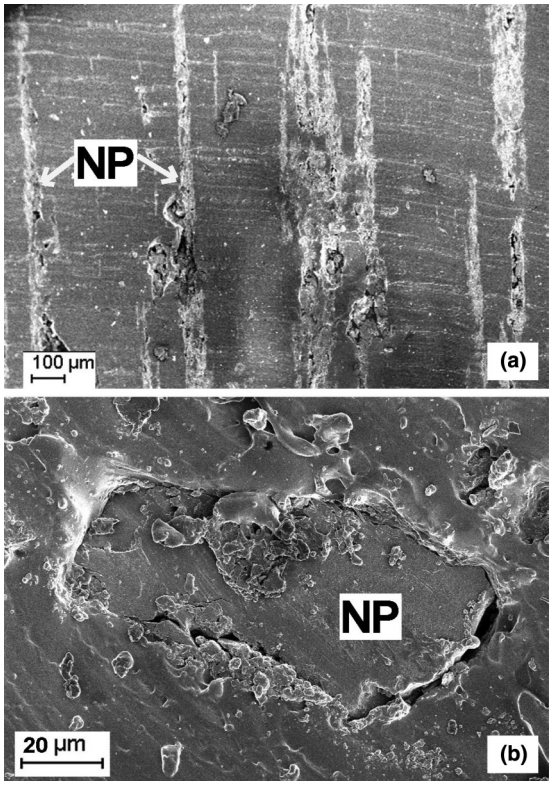

FIG. 1. Scanning electron microscopy images of the structured PDMS-Fe_3O_4 composites. The upper panel (a) shows a lateral view of the needles formed by magnetite nanoparticles in a 15% w/w composite, after alignment in an external magnetic field. The bottom panel (b) is a top view of one the inorganic needles in which a noncircular cross section (with aspect ratio $r = b/c$) can be observed.

This fact will be important when describing the angular variation of the FMR spectra for different directions of the applied magnetic field. Due to their very small volume, individual magnetite particles are superparamagnetic at room temperature, and consequently they cannot reach saturation. Magnetization vs field loops give magnetization values $M \sim 50$ emu/gr and $M \sim 55$ emu/gr at 8 kOe and 12 kOe, respectively, which are approximately one-half of the room temperature saturation magnetization of bulk magnetite,[1] $M_s \sim 92$ emu/gr. Considering $\delta = 5.2$ gr/cm^3 the magnetization values at the given fields are then $M_s \sim 260$ emu/cm^3 and ~ 286 emu/cm^3. These values are similar to the magnetization reported[3] in nanoparticles of comparable size at the same fields.

Ferromagnetic resonance spectra have been acquired at room temperature with a commercial Bruker ESP 300 spectrometer at frequencies of 24 GHz (K band) and 34 GHz (Q band). The samples were cut in slabs of approximately 2 mm $\times$ 2 mm and a thickness of a fraction of a millimeter. Two different cuts were made from the original sample, trying to maintain the needles laying within or perpendicular to the surface of the slab. The samples were placed at the center of a resonant cavity where the derivative of the absorbed power was measured using a standard field modulation and lock-in detection technique with amplitudes in the range 5–20 Oe. The slab plane could be either parallel or perpendicular to the excitation microwave field, according to the desired angular variation. Angular variations with respect to the external dc field were made around the slab normal or within the slab plane. The maximum available dc field was 19 kOe.

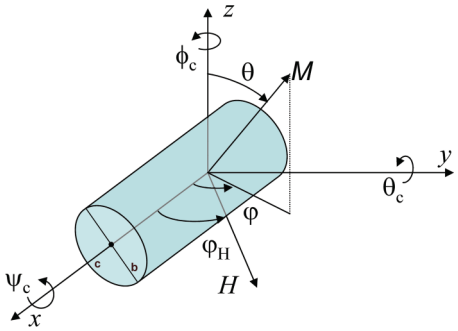

FIG. 2. (Color online) Schematics of the different vectors and angles involved in the description on the free energy. Cylinders (formed by the agglomeration of nanoparticles) are assumed to be on average aligned with the x axis, so that both θ_c and ϕ_c are almost zero, but ψ_c can vary randomly in the range $[0 - 2\pi]$. Slabs containing the cylinders can be in the xy plane (in-plane geometry) or in the yz plane (out-of-plane configuration). The cross section of the cylinder may have an ellipticity given by $r = b/c$.

III. EXPERIMENTAL RESULTS AND MODEL

Room temperature FMR measurements were made in 5% and 15% Fe_3O_4:PDMS samples at both K band and Q band frequencies. The external applied field was rotated from the direction of alignment of the needles to a perpendicular axis in order to study the magnetic anisotropy of the composite. We show schematically in Fig. 2 the vectors and angles that will be used in the expression of the free energy for a single cylinder. As we will see later, interactions among needles do not seem to be significant, so that the measured spectra can be described as the superposition of individually resonating entities. The average orientation of the cylinders formed by the magnetite nanoparticles is always assumed to be parallel to the x axis, the direction where the curing field was applied. The magnetic field $\tilde{\mathbf{H}}$ for the FMR experiment is rotated in the xy plane and characterized by the angle φ_H and the vector $\tilde{\mathbf{M}}$ is given by the polar and azimuthal angles θ and φ, respectively. In one of the used geometries (which we will call in-plane), the slab is placed in the xy plane so that the field variation tests the anisotropy within the slab. In the other geometry (called out-of-plane) we placed the sample in the xz plane to consider the anisotropy perpendicular to the slab. These experiments were made in order to account for possible dipolar interactions among cylinders which can give an effective demagnetization factor related to the shape of the slab. Cylinders are not necessarily aligned parallel to a single axis as determined in the observation of scanning electron microscopy (SEM) micrographs (see Fig. 1). It is then necessary to use the angles ψ_c, θ_c, and ϕ_c to account for possible misalignments of the needles and different orientations of the cylinder elliptical cross section with respect to the applied magnetic field. The angles θ_c and ϕ_c are assumed to be close to zero, while ψ_c can, in principle, vary randomly in the range $[0, 2\pi]$.

We show in Fig. 3 the K band FMR spectra of 5% Fe_3O_4:PDMS samples measured for different angles between

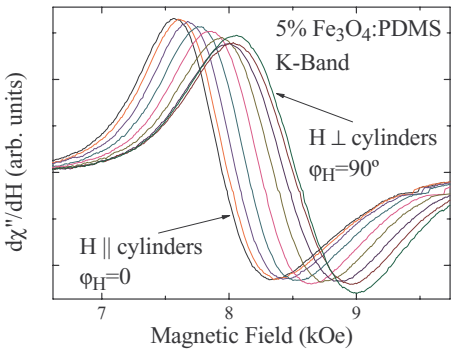

FIG. 3. (Color online) FMR spectra of 5% Fe_3O_4:PDMS as a function of the angle between the external field and the direction of alignment of the cylinders. Data have been measured at 300 K at K band. Spectra at Q band are similar, but with a center field around 11.8 kOe.

the external field and the direction of alignment of the cylinders in the elastomer. We defined $\varphi_H = 0$ as the angle when H is parallel to the needles. Spectra for other samples or frequencies are relatively similar, so we show only these data as an example of the overall observed behavior. The following main features can be seen in the spectra.

(i) The resonance field, H_r, is minimum when H is applied parallel to the long axis of the cylinders and maximum in the perpendicular direction, giving a 180° symmetry. This fact is a strong indication that curing the composite in the presence of an external field produces an easy magnetization axis parallel to the cylinders.

(ii) The difference between these two fields is almost independent of frequency and varies slightly with the geometry (in-plane or out-of-plane), indicating that interactions among cylinders are relatively low and affect only marginally the FMR response. We have observed a small dependence with the filler concentration, with the difference $H_{r\perp}(\varphi_H = 90^\circ) - H_{r\parallel}(\varphi_H = 0^\circ)$ being larger for the 5% sample. It is then possible to use a model of individual resonating entities to explain the observed spectra. However, changes in H_r are considerably lower than those expected from a simple model of a perfectly aligned group of cylinders, for which an upper limit[9] of $H_{r\perp} - H_{r\parallel}$ due to the shape anisotropy is given by $(3/2)2\pi M_s$. This estimation can be obtained from the appropriate expressions for H_r in uniaxial systems in the limit of low anisotropy compared to the resonance field, $H_{r\perp} = \omega/\gamma + \pi M_s$ and $H_{r\parallel} = \omega/\gamma - 2\pi M_s$. In our case this yields $H_{r\perp} - H_{r\parallel} \sim 2500$ Oe, using an average reduced value for $M_s = 265$ emu/cm^3. The observed experimental value of $H_{r\perp} - H_{r\parallel} \sim 600$ Oe is considerable lower than that expected from the mentioned simple model, indicating that the effective shape anisotropy of the composite could not be described as that of a perfect homogeneous cylinder.

(iii) The linewidth is also anisotropic, the maximum value of ΔH is found for $\varphi_H = 90^\circ$ and the minimum may occur at $\varphi_H = 0$ or at an intermediate angle, depending on the magnetite concentration in the composite. Frequency does not influence this behavior. To explain this variation it is necessary to take into account the ellipticity in the cross section of the needles and possible fluctuations in the shape anisotropy.

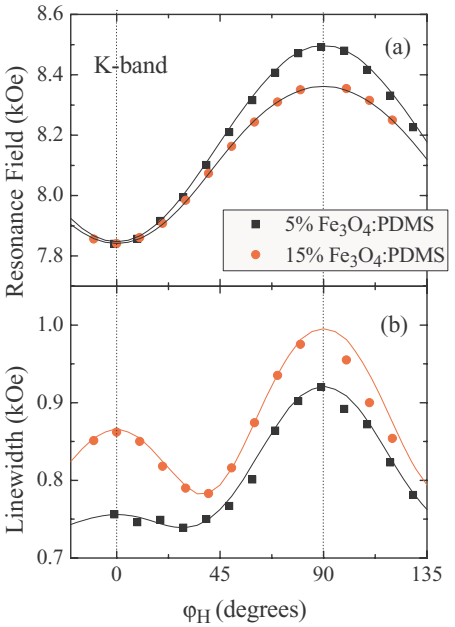

FIG. 4. (Color online) Resonance field (a) and peak to peak linewidth (b) taken from the experimental data of 5% and 15% Fe_3O_4:PDMS samples as a function of the angle between the external field and the direction of alignment of the cylinders. In this case the direction of alignment of the cylinders is within the PDMS slab (in-plane geometry). The corresponding spectra were measured at 300 K and at K band (24 GHz). The continuous line are best fits obtained from the proposed model and the parameters given in Table I.

(iv) The line shape is almost symmetrical, but the low field part is somewhat higher and narrower than the high field part. This observation suggests that additional effects, such as magnetocrystalline anisotropy, should be accounted for in order to fully describe the observed experimental behavior. These effects will be further discussed and explained when the cubic anisotropy term is considered in the model.

Figures 4 and 5 show the angular variation of the resonance field and the linewidth extracted from the measured spectra for the two filler concentrations at 24 GHz and 34 GHz. As already stated differences between the two samples are relatively small but, as we will show later, can be understood within a mean field model that includes fluctuations in the anisotropy parameters. The almost sinusoidal dependence of the angular variation of the resonance field at K and Q bands is consistent with an effective anisotropy field considerable lower than the working frequency in units of field. In uniaxial systems the anisotropy is $H_A \sim 2/3\,(H_{r\perp} - H_{r\parallel})$ which yields $H_A \sim 400$ Oe for our samples, while the expected resonance fields are around 8500 Oe and 12000 Oe for K and Q bands, respectively, for $g \sim 2$.

To explain the observed behavior we have used the Smit and Beljers[10] formalism to calculate the resonant modes, starting with a free energy that considers the Zeeman effect, the cubic magnetocrystalline anisotropy, and the cylindrical shape of the needles,

$$F = -\tilde{\mathbf{M}} \cdot \tilde{\mathbf{H}} + K_c\left(\alpha_1^2\alpha_2^2 + \alpha_2^2\alpha_3^2 + \alpha_3^2\alpha_1^2\right) + \tfrac{1}{2}\tilde{\mathbf{M}} \cdot \mathbf{N} \cdot \tilde{\mathbf{M}}. \quad (1)$$

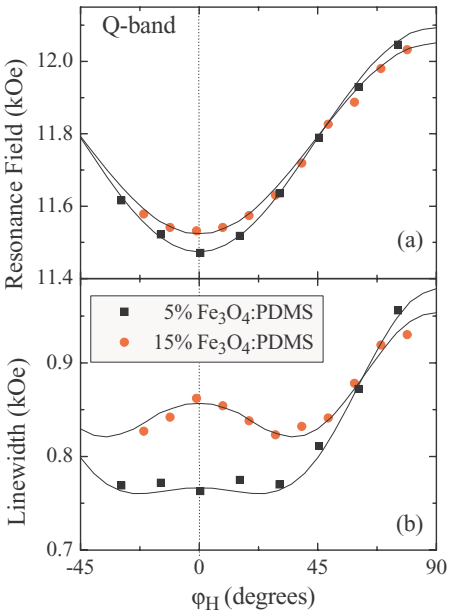

FIG. 5. (Color online) Room temperature Q-band resonance field (a) and linewidth (b) for 5% and 15% Fe_3O_4:PDMS samples as a function of the angle between the external field and the direction of alignment of the cylinders which, in this case, was perpendicular to the PDMS slab (out-of-plane geometry). The continuous lines are best fits obtained from the proposed model and the parameters reported in Table I.

In a fixed coordinate system the magnetization vector is given by $\tilde{\mathbf{M}} = M(\cos\varphi\,\sin\theta, \sin\varphi\,\sin\theta, \cos\theta)$ and the external field $\tilde{\mathbf{H}} = H(\cos\varphi_H, \sin\varphi_H, 0)$ is assumed to rotate in the xy plane. K_c is the cubic magnetocrystalline anisotropy, which for bulk magnetite[1] is $K_c \sim -1.35 \times 10^5$ emu/cm^3, and α_i are the directional cosines. We will leave for the moment the discussion of the effects of the magnetocrystalline anisotropy of the individual grains forming the needles and discuss first the shape effects. If long enough circular cylinders were aligned parallel to the x axis, the demagnetization tensor $\mathbf{N}$ would be diagonal with elements $N_{xx} = 0$, $N_{yy} = N_{zz} = 2\pi$. However, the needles are composed by an agglomeration of individual particles so that the demagnetization factors could differ considerable from these values. To treat this situation[11–14] a shape parameter P is often used, with $P = 1$ for perfectly homogeneous cylinders formed by closely packed spherical nanoparticles, and $P = 0$ if the particles (assumed spherical) are far apart so that the dipolar interaction does not contribute to the shape. Intermediate values of P serve to quantify the "cylindricity" of the needles. Taking into account the shape factor, the demagnetization tensor is still diagonal, but now it has the values $N_{xx} = \frac{4}{3}\pi(1-P)$, $N_{yy} = N_{zz} = \frac{4}{3}\pi(1 + P/2)$. As expected, for $P = 1$ we recover the shape factors for a perfect cylinder and for $P = 0$ we obtain the demagnetization factors for a sphere. We mentioned that the cylinder cross section is elliptical rather than circular, so that if $r = b/c$ is the ratio between the two axes, the resultant tensor elements are $N_{xx} = \frac{4}{3}\pi(1-P)$, $N_{yy} = \frac{4}{3}\pi(1 + P/2)2/(r+1)$, and $N_{zz} = \frac{4}{3}\pi(1 + P/2)2r/(r+1)$. In a real sample the long axis of the needles is not necessarily aligned with the x axis, so that in the fixed reference frame the demagnetization tensor $\mathbf{N}_f$ will not remain diagonal. If $\mathbf{N}_d$ is the diagonal demagnetization tensor, the relationship between both is

$$\mathbf{N}_f = \mathbf{R}\mathbf{N}_d\mathbf{R}^{-1}, \tag{2}$$

where $\mathbf{R} = \mathbf{R}_x\mathbf{R}_y\mathbf{R}_z$ is the rotation matrix composed of three consecutive anticlockwise rotations by angles ϕ_c, θ_c, and ψ_c around the axis z, y, and x, respectively, as shown in Fig. 2. With this election the angles ϕ_c, θ_c can be used to localize the long axis of the cylinder, while ψ_c gives the orientation of b, the larger axis of the elliptical cross section of the cylinder. It is possible to find complete expressions for $\mathbf{N}_f$ for any values of the three angles, but we are assuming that the needles are mostly parallel to the x axis, so that approximate expressions may be used for $\phi_c \sim \theta_c \sim 0$. In this case we obtain

$$\mathbf{N}_f = \begin{pmatrix} N_{xx} & N_{xy} & N_{xz} \\ N_{yx} & N_{yy} & N_{yz} \\ N_{zx} & N_{zy} & N_{zz} \end{pmatrix}, \tag{3}$$

with

$$\begin{aligned}
N_{xx} &= \frac{4}{3}\pi(1-P) = 4\pi - N_{yy} - N_{zz}, \\
N_{yy} &= \frac{4\pi}{3(1+r)}[(2+P)(r+(1-r)\cos^2\psi_c) \\
&\quad -(1+2P+r-rP)\theta_c\phi_c\sin 2\psi_c], \\
N_{zz} &= \frac{4\pi}{3(1+r)}[(2+P)(1+(r-1)\cos^2\psi_c) \\
&\quad +(1+2P+r-rP)\theta_c\phi_c\sin 2\psi_c], \\
N_{xy} &= N_{yx} = \frac{4\pi}{3(1+r)}[(1-P-r-2rP)\theta_c\sin\psi_c \\
&\quad -(1+2P+r-rP)\phi_c\cos\psi_c], \\
N_{xz} &= N_{zx} = \frac{4\pi}{3(1+r)}[-(1-P-r-2rP)\theta_c\cos\psi_c \\
&\quad -(1+2P+r-rP)\phi_c\sin\psi_c], \\
N_{yz} &= N_{zy} = \frac{4\pi}{3(1+r)}[(2+P)(1-r)\sin\psi_c\cos\psi_c \\
&\quad +(1+2P+r-rP)\theta_c\phi_c\cos 2\psi_c].
\end{aligned} \tag{4}$$

The explicit form for the free energy of Eq. (1) (without the cubic term) is then

$$\begin{aligned}
F &= -MH\,\cos(\varphi-\varphi_H)\sin\theta \\
&\quad +\tfrac{1}{2}M^2[\sin^2\theta(N_{xx}\cos^2\varphi + N_{yy}\sin^2\varphi) \\
&\quad +N_{zz}\cos^2\theta + N_{xy}\sin^2\theta\,\sin 2\varphi \\
&\quad +\sin 2\theta(N_{xz}\cos\varphi + N_{yz}\sin\varphi)].
\end{aligned} \tag{5}$$

From this expression for the free energy, it is possible to calculate the angular derivatives evaluated at the equilibrium

angles,

$$\begin{aligned}
\frac{\partial^2 F}{\partial\theta^2} &= M\left[\begin{array}{c} H\ \cos(\varphi-\varphi_H)\sin\theta - 2M\ \sin 2\theta(N_{xz}\cos\varphi + N_{yz}\sin\varphi) \\ +M\ \cos 2\theta(N_{xx}\cos^2\varphi + N_{yy}\sin^2\varphi + N_{xy}\sin 2\varphi - N_{zz})\end{array}\right],\\
\frac{\partial^2 F}{\partial\varphi^2} &= M\left[\begin{array}{c} H\ \cos(\varphi-\varphi_H)\sin\theta - \frac{M}{2}\sin 2\theta(N_{xz}\cos\varphi + N_{yz}\sin\varphi) \\ -M\ \sin^2\theta(2N_{xy}\sin 2\varphi + (N_{xx}-N_{yy})\cos 2\varphi)\end{array}\right],\\
\frac{\partial^2 F}{\partial\theta\partial\varphi} &= M\left[\begin{array}{c} \sin(\varphi-\varphi_H)\cos\theta + M\ \cos 2\theta(N_{yz}\cos\varphi - N_{xz}\sin\varphi) \\ +\frac{M}{2}\sin 2\theta(2N_{xy}\cos 2\varphi + (N_{yy}-N_{xx})\sin 2\varphi)\end{array}\right].
\end{aligned} \tag{6}$$

Replacing Eqs. (4) and (6) in the Smit and Beljers[10] formulas,

$$\left(\frac{\omega}{\gamma}\right)^2 = \frac{1}{M^2\sin^2\theta}\left[\frac{\partial^2 F}{\partial\theta^2}\frac{\partial^2 F}{\partial\varphi^2} - \frac{\partial^2 F}{\partial\theta\partial\varphi}\right], \tag{7}$$

$$\frac{\Delta\omega}{\gamma} = \frac{\alpha}{2M}\left(\frac{\partial^2 F}{\partial\theta^2} + \frac{1}{\sin^2\theta}\frac{\partial^2 F}{\partial\varphi^2}\right), \tag{8}$$

it is possible to arrive at the dispersion relation and the damping expression for the resonance modes. In the above expression $\gamma = g\mu_B/\hbar$, with μ_B the Bohr magneton.

The parameters involved in the model are the magnetization (M), the g value, the damping parameter (α), the shape factor (P), and the cross section ratio of the cylinders (r). Each of these parameters modifies the resonance spectra (mostly) in the following ways: the g value is related to the "center of gravity" of the angular variation of the resonance field. The magnetization M is proportional to the maximum difference between the resonance field perpendicular and parallel to the axis of the needle. As already mentioned, in systems with relatively low anisotropy[9] compared with ω/γ, which holds in this case for both frequencies, $H_{r\perp} - H_{r\parallel} \sim 3\pi M$. As the measured difference is around 1/4 smaller than the expected value, the factor P is introduced to account for the reduced anisotropy compared to that of a perfect cylinder.

To explain the angular variation of the linewidth, ΔH, we need to consider at least the following effects: one is the elliptical cross section, which is assumed to be randomly oriented with respect to the axis of the cylinder, giving a minimum parallel to the cylinder axis and a maximum in the perpendicular orientation. Another effect arises from possible fluctuations in the shape parameter, P, which tends to increase ΔH mainly in the direction parallel to the easy axis. The misalignment of the cylinders with respect to the easy direction also contributes to an enhancement the linewidth.

There are numerous reports[3,6,15–18] of the FMR linewidth in Fe_3O_4, spanning from $\Delta H \sim 150$ Oe[17] to 1500 Oe.[15,18] In most cases the origin of a broadened line is due to extrinsic or inhomogeneous contributions, so that the measured peak to peak linewidth for Lorentzian-like lines is usually written as the sum of an intrinsic term (which in a first approximation increases linearly with frequency) and a frequency independent contribution, $\Delta H \sim (2/\sqrt{3})\alpha\omega/\gamma + \Delta H_0$. From the lowest reported value[17] for the linewidth at X- band ($\nu \sim 9.5$ GHz) it is possible to estimate $\alpha \lesssim 0.04$ for the intrinsic damping parameter. As can be seen in Figs. 4 and 5 the linewidth is almost the same for K and Q bands indicating that the line broadening in our samples arises mainly from the inhomogeneous contribution. Because the needles are formed by a collection of randomly oriented individual nanoparticles, a contribution to the linewidth due to the sum of particles resonating at different fields must be taken into account. Note also that the magnitude of M and K_c can vary from particle to particle which will also change the linewidth and the line shape. All these variables affect the FMR spectrum in different ways and could be taken into account with appropriate models,[9,19] but in a first approximation it is enough to consider the random distribution of cubic magnetocrystalline axes to account for the average linewidth and the asymmetry in the line shape.

We have made computer simulations of the FMR spectra of a set of randomly oriented nanoparticles for the cases of a positive or a negative cubic magnetocrystalline anisotropy field, H_c. The first case corresponds to materials like Fe, in which the easy axes are parallel to the ⟨100⟩ directions. Magnetite, on the other hand, has negative anisotropy indicating that the directions of easy magnetization are aligned with the ⟨111⟩ axes. In Fig. 6 we show the expected spectrum for both cases. It can be seen that although the particles are randomly oriented the line shape is not symmetric, similar to the observed behavior in uniaxial systems[20] with positive or negative anisotropy. In particular, negative cubic anisotropy produces an asymmetry in which the low field part of the line is narrower and higher than the high field region. The opposite behavior is predicted for materials with positive cubic anisotropy. We have already shown (see Fig. 3) that the composites have slightly asymmetric resonant lines, which are then compatible with the predictions made for negative H_c,

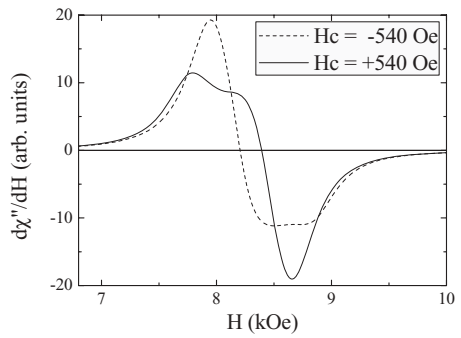

FIG. 6. Simulated spectra of materials with cubic magnetocrystalline anisotropy composed of randomly oriented particles. For the simulation we have used $M = 265$ emu/cm^3, $H_c = \pm 540$ Oe, $g = 2.055$, $\alpha = 0.06$, $\omega = 24$ GHz, and averaged the spectra of 30 000 individual particles.

as expected for Fe $_3O_4$. The asymmetry in the experimental spectra is lower than that of the simulated results, suggesting that fluctuations in M, H_c or even a nonrandom distribution of the anisotropy axes should be taken into account. However, in the case of negative cubic anisotropy, the magnetocrystalline effects do not predict an angular variation of the resonant field and linewidth[21] that matches the observed behavior, even if a nonrandom distribution of crystalline axes is assumed. This prediction indicates that the cubic axes are at random and the most important anisotropy effects are produced by the shape and the elliptical cross section of the cylinders.

For the above-mentioned reasons the effects of the magnetocrystalline anisotropy can be included in an effective linewidth which we have chosen to match the observed value parallel to the needle axis, $\Delta H_{\parallel} \sim 750$ Oe. At K band this yields an effective alpha value $\overline{\alpha} \sim 0.13$. As we are assuming $\Delta H = 2/\sqrt{3}\,\overline{\alpha}\frac{\omega}{\gamma}$ and the measured linewidth does not change with frequency, the value of $\overline{\alpha}$ should be frequency dependent. From this value of $\overline{\alpha}$ it is possible to estimate the damping constant $\alpha = \overline{\alpha} - \sqrt{3}/2\Delta H/\frac{\omega}{\gamma} \sim \overline{\alpha} - \sqrt{3}/2\Delta H_0/\frac{\omega}{\gamma}$, which holds when $\Delta H \sim \Delta H_0$, i.e., when the major contribution to the linewidth is due to inhomogeneous broadening.

To simulate the angular variation of H_r and ΔH we have used a Lorentzian-like line shape that can be deduced from the scalar magnetic susceptibility (which gives the microwave response of the system to the microwave perturbation field). Following Refs. 11 and 22, χ can be written as

$$\begin{aligned}\chi &= \chi' + i\chi'' \\ &= \frac{1+\overline{\alpha}^2}{\left(\frac{\omega}{\gamma}\right)^2 - \left(\frac{\omega_0}{\gamma}\right)^2 + i\frac{\omega_0}{\gamma}\frac{\Delta\omega}{\gamma}}\left[l^2\left(\frac{\partial^2 F}{\partial\theta^2} + i\alpha'\right)\right. \\ &\quad \left. + m^2\left(\frac{1}{\sin^2\theta}\frac{\partial^2 F}{\partial\varphi^2} + i\alpha'\right) + 2lm\frac{\partial^2 F}{\partial\theta\partial\varphi}\frac{1}{\sin\theta}\right], \qquad (9)\end{aligned}$$

with $\omega_0/2\pi = \nu$ the microwave excitation frequency, $\alpha' = \frac{\omega_0}{\gamma}M\frac{\overline{\alpha}}{1+\overline{\alpha}^2}$, and $l = 0, m = -\sin\theta$ when the microwave field is applied in the z direction (as in the present case). The absorbed power is proportional to χ'', the imaginary part of the scalar susceptibility, and hence the line shape can be written as

$$\chi''(\omega) = -\frac{\omega_0}{\gamma}\frac{\overline{\alpha}\left[\left(\frac{\omega}{\gamma}\right)^2 - \left(\frac{\omega_0}{\gamma}\right)^2\right]M\,\sin^2\theta - (1+\alpha^2)\frac{\Delta\omega}{\gamma}\frac{\partial^2 F}{\partial\varphi^2}}{\left[\left(\frac{\omega}{\gamma}\right)^2 - \left(\frac{\omega_0}{\gamma}\right)^2\right]^2 + \left(\frac{\omega_0}{\gamma}\frac{\Delta\omega}{\gamma}\right)^2}. \qquad (10)$$

To obtain the average susceptibility it is necessary to integrate χ'' in the angular variables ψ_c (which is chosen to have a random distribution in the interval $[0, 2\pi]$), θ_c, and ϕ_c and other parameters which could have a variation around an average value. For θ_c, ϕ_c, P, and r we have assumed a Gaussian distribution centered at an average value with a width $\sigma\theta_c, \sigma\phi_c, \sigma P$, and σr. Other sources of line broadening are included in the $\overline{\alpha}$ parameter.

The FMR response was simulated by adding a minimum of 5×10^4 spectra in which the angular variables and the free parameters were generated with their corresponding distribution functions. This number of spectra was found to be enough to converge to an average spectrum in which the addition of more spectra did not change significantly the line shape. The initial field for each spectrum always started at 0 Oe and the maximum field was varied depending on the values of the parameters used in the simulation. This field was chosen large enough so that a negligible absorption was computed for fields above this value, and 20 kOe was found to be enough in most cases. When evaluating the spectra the total field span was divided in 1200 steps. The value of M was estimated from the magnetization measurements as a function of the applied field reported in Ref. 7. We observed a small field dependence which gives $M = 265$ emu/cm^3 for K-band fields ($H \sim 8500$ Oe) and $M = 290$ emu/cm^3 for Q band ($H \sim 12000$ Oe). Due to the superparamagnetic nature of the particles at room temperature the magnetization is not completely saturated at the fields where the absorptions are observed. Thermal effects are usually introduced into the free energy, Eq. (1), by replacing different powers of M by their corresponding expressions corrected by thermal fluctuations.[23] In the present case M must be replaced by $M_s L_1(x)$ and M^2 by $M_s^2 L_2(x)$, with $x = \mu H/k_B T$, $L_1(x) = \coth(x) - 1/x$, and $L_2(x) = 1 - 3L_1(x)/x$. For our samples the resonant fields are always larger than 8 kOe and in this field region $L_2(x) \sim L_1^2(x)$. With this approximation all powers of $M(H,T)$ in Eq. (1) should be replaced by the corresponding power of $M_s L_1(x)$ which, for a fixed temperature, is equivalent to using the value of $M(H)$ from the hysteresis loop.

The rest of the parameters (P, g, $\overline{\alpha}$, and r) were varied until a reasonable fit of the angular variations of Figs. 4 and 5 was obtained. In a first approach $\sigma\theta_c$, $\sigma\phi_c$, σP, and σr were fixed to zero and only one of them was allowed to change in order to analyze how fluctuations influence the angular variations.

In Fig. 7 we present simulations for the angular variation of ΔH as a function of the angle φ_H between the external field and the x axis with the parameters indicated in the figure caption. Angular variations of H_r (not shown) are almost unaffected by Gaussian fluctuations in P, θ_c, ϕ_c, or r. This is not unexpected because the average value of H_r does not change if the distribution function is symmetric. In Fig. 7(a) we show the effects of a Gaussian distribution of the shape parameter P with a width σP. Changes in ΔH are strongly dependent on the value of σP, especially when the field is applied parallel to the easy axis of the cylinder. For $\sigma P = 0$ the linewidth grows monotonically with the angle φ_H, but for $\sigma P > 0$ the width $\Delta H_{\parallel}$ increases considerably, and the minimum occurs at an intermediate angle. The differences between the easy and the hard axes are essentially due to the nonuniformity of Eq. (7) as a function of φ_H, yielding in general a maximum linewidth when $\varphi_H = 0$, a minimum at an intermediate angle, and a relative maximum along the hard axis.[21] In this special case, the random orientation of ψ_c for a fixed value of $r = b/c$ gives the largest contribution to ΔH for $\varphi_H = 90^\circ$, and hence the effect of σP is less important in this direction. This correction seems to be enough to explain the angular variation of Figs. 4 and 5 with values of $\sigma P \sim 0.1$–0.3, particularly for the samples with larger Fe_3O_4 concentration.

In Fig. 7(b) we show the effects of changing the aspect ratio of the cylinders while keeping other parameters fixed. It is observed that increasing r broadens $\Delta H_{\perp}$ and, as expected, produces no changes in $\Delta H_{\parallel}$. We have also simulated the influence of fluctuations in the parameter r by an amount σr in the range $0 \leqslant \sigma r \leqslant 0.6$ and found that

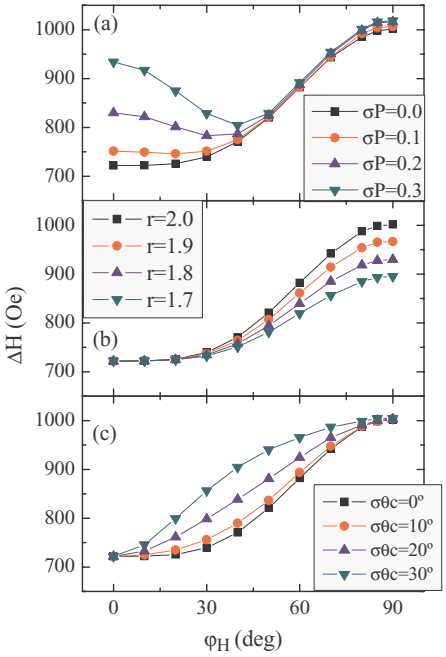

FIG. 7. (Color online) Angular variation of the linewidth when fluctuations in different parameters are allowed. For the simulations we have used $\omega/2\pi = 24$ GHz, $M = 265$ emu/cm^3, $g = 2.055$, $\alpha = 0.15$, $P = 0.6$, $\sigma P = 0$, $r = 2$, $\theta_c = \phi_c = 0$, $\sigma\theta_c = \sigma\phi_c = 0$, ψ_c random in $[0, 2\pi]$, and averaged the spectra of 50 000 individual particles. Panel (a) shows the effects of a Gaussian distribution of width $\sigma P \geqslant 0$ on ΔH; in panel (b) the influence of different values of r is analyzed, and in panel (c) we present the influence of a Gaussian distribution of width $\sigma\theta_c = \sigma\phi_c$ on the linewidth.

the angular variations of the resonant field and the linewidth remain almost unaffected. This implies that fluctuations in the cross section of the cylinders (which are effectively observed in SEM micrographs) will not reflect in the line shape if the perpendicular axes of the needles are randomly distributed.

The other effect that we have considered is the misalignment of the cylinders with respect to the x axis. To account for this correction the angles θ_c and ϕ_c are assumed to be Gaussian distributed around zero with the same dispersion, $\sigma\theta_c = \sigma\phi_c$. Again this contribution produces little changes on the curves H_r vs φ_H but, as shown in Fig. 7(c), the linewidth tends to increase at intermediate angles. This behavior is a consequence of the dependence of the linewidth with $|\partial H_r/\partial\theta_c|$ (and $|\partial H_r/\partial\phi_c|$) which tends to be zero for H parallel or perpendicular to the easy axis and maximum at an intermediate angle.[21] Note, however, that the values of $\sigma\theta_c$ and $\sigma\phi_c$ should be considerably large ($\sigma\theta_c \geqslant 20^\circ$) in order to produce a significant variation in ΔH.

To summarize the results predicted by the computational simulations on the angular variation of the linewidth, we have found that (i) fluctuations in the shape factor P increase $\Delta H_\parallel$ considerably and do not modify $\Delta H_\perp$ appreciably. (ii) Different values of r only change ΔH close to the normal to the cylinders. (iii) The misalignment of the needles enhances the linewidth at intermediate angles, but relatively large values of $\sigma\theta_c$ and $\sigma\phi_c$ are needed to produce significant effects.

TABLE I. Parameters used to fit the angular variations of H_r and ΔH in Figs. 4 and 5. The frequencies are $\nu = 23.95$ GHz and $\nu = 34.0$ GHz for K and Q bands, respectively.

Sample/frequency	M(emu/cm^3)	g	P	σP	$\overline{\alpha}$	r	$\sigma\theta$
15% K band	265	2.074	0.534	0.28	0.129	2.2	0
5% K band	265	2.055	0.590	0.13	0.127	1.8	0
15% Q band	290	2.038	0.506	0.18	0.100	1.8	0
5% Q band	290	2.037	0.552	0.10	0.093	1.9	0

In Table I we present the parameters we have used to fit the angular variations of Figs. 4 and 5. A very good agreement is obtained for both the resonance field and the linewidth in the two samples and frequencies. For both frequencies it is observed that the 5% sample has P values approximately 10% larger than the more concentrated elastomer. This probably originates in the already mentioned higher length/diameter aspect ratio of the diluted samples which is compatible with a larger value of P. Values of σP also differ in the two samples, being larger in the 15% composite by a factor of 2. This is indicating that, as the concentration increases, the cylinders tend to form with higher variations in their aspect ratio.

The cross section aspect ratio r has an average value $\langle r\rangle \sim 1.9$ very similar to what it is observed in SEM pictures. The present measurements are not adequate to account for possible fluctuations in this parameter, which are indeed present in the samples. The value of $\overline{\alpha}$ is almost the same for both samples, but shows an appreciable variation with frequency. If we consider that the intrinsic damping parameter $\alpha \sim \overline{\alpha} - \sqrt{3}/2\Delta H_0/\frac{\omega}{\gamma}$, the estimated values are in the range $\alpha \sim 0.04$–0.05, which are quite similar to the reports made for high quality films.[17] We also found that it was not necessary to consider possible fluctuations in the alignment of the needles with respect to the x axis. Although in a direct view of the needles it is possible to observe that they are not perfectly aligned in a unique direction; the variance of the normal distribution around the curing direction is less than 5° in both dilutions. As simulations show that a value of $\sigma\theta_c \gtrsim 20^\circ$ is needed to produce measurable effects in the angular variations of the linewidth, this effect could hardly be noticed in our samples. The g values are somewhat smaller that those generally accepted in the literature which span[15,16,24] in the range $g = 2.09$–2.14. Although there are reports[25] of g values as low as $g = 1.985$, the reduction in this parameter most probably arises in the difficulty to assure an alignment of the average easy axis of the cylinders parallel to a given orientation (the x axis in the fixed reference frame). In this situation there is a reduced number of cylinders parallel to the direction defined as "easy"and then the overall spectrum tends to move to larger fields given a lower g value. Also, extra care should be taken with the estimation of the g value when the lines are not symmetric, as in the simulations of Fig. 6 for a random collection of particles with cubic anisotropy. If one defines the resonance field as the zero crossing (or even worse the field at half height), the estimated g value from the spectra is $g \sim 2.09$ for negative anisotropy and $g \sim 2.04$ for positive H_c, while the value used for the simulations was $g \sim 2.055$.

IV. CONCLUSIONS

We have shown that FMR is a very powerful technique to get deeper information on the magnetic microstructure of magnetorheological elastomers composed of aligned cylinders. Using a model that considers a shape factor and the ellipticity in the cross section of the needles, it was possible to fit the angular variations of the resonance field and linewidth at different frequencies and for samples of different filling concentrations. In the case of r the calculated parameters are in good agreement with direct images obtained by SEM, which show an ellipticity in the cross section of the needles. The values of P and σP are also compatible with the observations of a higher aspect ratio in cylinders with a lower filling concentration.

ACKNOWLEDGMENTS

This work was supported in part by Conicet under Grant No. PIP 112-200801-00245, ANPCyT under Grant No. PICT 2010-0773, and U.N. Cuyo under Grant No. 06/C352, all from Argentina. Fruitful discussions with Dr. Carlos A. Ramos and technical support from Rubén E. Benavides are greatly acknowledged.

*butera@cab.cnea.gov.ar; also at Consejo Nacional de Investigaciones Científicas y Técnicas and Instituto de Nanociencia y Nanotecnología, Argentina.

[1] J. M. D. Coey, *Magnetism and Magnetic Materials* (Cambridge University Press, Cambridge, UK, 2010).
[2] A. G. Roca, M. P. Morales, K. O'Grady, and C. J. Serna, Nanotechnology **17**, 2783 (2006).
[3] G. F. Goya, T. S. Berquó, F. C. Fonseca, and M. P. Morales, J. Appl. Phys. **94**, 3520 (2003).
[4] J. M. Vargas, E. Lima, R. D. Zysler, J. G. S. Duque, E. De Biasi, and M. Knobel, Eur. Phys. J. B **64**, 211 (2008).
[5] D. M. Lind, S. D. Berry, G. Chern, H. Mathias, and L. R. Testardi, Phys. Rev. B **45**, 1838 (1992).
[6] J. M. Vargas, J. Gómez, R. D. Zysler, and A. Butera, Nanotechnology **18**, 115714 (2007).
[7] J. L. Mietta, M. M. Ruiz, P. S. Antonel, O. E. Pérez, A. Butera, G. Jorge, and R. M. Negri, Langmuir **28**, 6985 (2012).
[8] P. S. Antonel, G. Jorge, O. E. Pérez, A. Butera, A. G. Leyva, and R. M. Negri, J. Appl. Phys. **110**, 043920 (2011).
[9] A. Butera, Eur. Phys. J. B **52**, 297 (2006).
[10] J. Smit and H. G. Beljers, Philips Res. Rep. **10**, 113 (1955).
[11] U. Netzelmann, J. Appl. Phys. **68**, 1800 (1990).
[12] A. Butera, J. N. Zhou, and J. A. Barnard, Phys. Rev. B **60**, 12270 (1999).
[13] J. Gómez, A. Butera, and J. A. Barnard, Phys. Rev. B **70**, 054428 (2004).
[14] M. Spasova, U. Wiedwald, R. Ramchal, M. Farle, M. Hilgendorff, and M. Giersig, J. Magn. Magn. Mater. **240**, 40 (2002).
[15] L. R. Bickford, Jr., Phys. Rev. **78**, 449 (1950).
[16] J. J. Krebs, D. M. Lind, and S. D. Berry, J. Appl. Phys. **73**, 6457 (1993).
[17] P. A. A. van der Heijden, M. G. van Opstal, C. H. W. Swiiste, P. H. J. Bloemen, J. M. Gaines, and W. J. M. de Jonge, J. Magn. Magn. Mater. **182**, 71 (1998).
[18] T. Bodziony, N. Guskos, J. Typek, Z. Roslaniec, U. Narkiewicz, and M. Maryniak, Rev. Adv. Mater. Sci. **8**, 86 (2004).
[19] A. Butera, S. S. Kang, D. E. Nikles, and J. W. Harrell, Physica B **354**, 108 (2004); A. Butera, J. L. Weston, and J. A. Barnard, J. Magn. Magn. Mater. **284**, 17 (2004).
[20] J. Curiale, R. D. Sánchez, C. A. Ramos, A. G. Leyva, and A. Butera, J. Magn. Magn. Mater. **320**, e218 (2008).
[21] A. Butera, J. Gómez, J. L. Weston, and J. A. Barnard, J. Appl. Phys. **98**, 033901 (2005).
[22] E. P. Valstyn, J. P. Hanton, and A. H. Morrish, Phys. Rev. **128**, 2078 (1962).
[23] E. De Biasi, C. A. Ramos, and R. D. Zysler, J. Magn. Magn. Mater. **262**, 235 (2003).
[24] B. Aktas, Thin Solid Films **307**, 250 (1997).
[25] Y. Köseoğlu and B. Aktaş, Phys. Status Solidi C **1**, 3516 (2004).